International Conference on Space Optics—ICSO 2022

Dubrovnik, Croatia

3–7 October 2022

Edited by Kyriaki Minoglou, Nikos Karafolas, and Bruno Cugny,

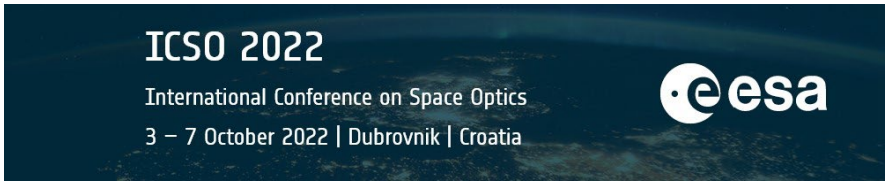

High dynamic range HgCdTe APD detector dedicated to LiDAR applications: design and test results

International Conference on Space Optics — ICSO 2022, edited by Kyriaki Minoglou, Nikos Karafolas, Bruno Cugny, Proc. of SPIE Vol. 12777, 127772C · © 2023 ESA and CNES · 0277-786X · doi: 10.1117/12.2689980

High dynamic range HgCdTe APD detector dedicated to LiDAR applications: design and test results

E. de Borniol*[a], J. Abergel [a], G. Badano [a], J.-A. Nicolas [a], J.-P. Rostaing [a], J. Rothman [a]
[a]Univ. Grenoble Alpes, CEA, LETI, F38000 Grenoble, France

ABSTRACT

LiDAR remote sensing of the atmosphere requires a photons detection chain with a high sensitivity and a high dynamic range associated with a good temporal resolution. To meet these requirements, a specific CMOS read out circuit (ROIC) has been studied, design and realized at CEA/Leti within the frame of the H2020 project HOLDON. This ROIC is based on a CTIA amplifier with four different current/voltage conversion gain thanks to capacitance ranging from 10 fF to 10 pf. Other functionalities like on chip sampling, auto-reset or programmable low pass filtering have been implemented to optimize the detector for different measurement chain. Based on this circuit architecture, two versions of the ROIC with different way to connect the circuit to the photodiodes have been manufactured and tested. The first one is design to be directly hybridized to a small array of photodiodes with a format imposed by the ROIC design in term of pixel pitch and array size. For the second ROIC version, the photodiode array is hybridized to an interconnection circuit used as a fan-out of electrical connections to a bonding pad. This module is then wire-bonded to the ROIC to get the final detector assembly. This configuration allows us to couple the ROIC with different APD geometry adapted to a specific application need. The performances of one of the first hybridized devices were previously presented during ICSO 2020[1]. For this review, we focus on the second version of the ROIC. The tested detector module is made of an array of 76 HgCdTe APD in parallel with a pixel pitch of 15 µm. The array forms a 150 µm diameter macro-photodiode. The device was tested at 78K within a liquid nitrogen cooled cryostat. Under photon flux, we have obtained a linear response of the device with an incoming flux varying over more than six orders of magnitude without varying the APD gain. This wild dynamic is associated with a high sensitivity with a noise standing below the unique photon. The response to a brief laser pulse gives a rise time ranging from 175 ns for the highest CTIA gain to 6 ns for the lowest CTIA gain.

Keywords: HgCdTe, APD, dynamic range, LiDAR, persistence

1. INTRODUCTION

LiDAR is a demanding application for photon detectors as it needs high sensitivity, high dynamic range with a good temporal resolution. With their exceptional performances as high linear gain, low multiplication noise and high quantum efficiency[1], HgCdTe or MCT (Mercury Cadnium Tellurium) APDs have demonstrated its ability to respond to these requirements. Nevertheless, a specific application needs for a specific photodiode and adapted CMOS circuit to extract the photocurrent. The development of such a detector dedicated to LiDAR systems was the aim of HOLDON H2020 European project (HgCdTe APD Optimization for Lidar Detection Of greeNhouse gas). For this project, a consortium of end-users, test bench developers and detector manufacturers has been settled to define the needs and then develop, realize and test a versatile detection chain dedicated to LiDAR applications. The detector module, comprising the HgCdTe avalanche photodiode (APD) and the dedicated CMOS read-out integrated circuit (ROIC), was developed at CEA Leti. ID Quantique has designed and fabricated the proximity electronic providing the control signals and data acquisition. The sets made up of these two main parts are being currently distributed to the end-user partners DLR, LMD and Airbus to be tested and/or implemented in full LiDAR systems, the final goal being to demonstrate the use of the detector in different LiDAR methods for greenhouse gases detection. Always in the frame of HOLDON project, a Near-infrared, visible and ultraviolet (NIR-VIS-UV) LiDAR echo emulator (LEE) has been developed by Alter technology[2][3]. The LEE will be used by Airbus to fully characterize two detector modules, the long-term goal being to have a detector that meets the requirements for most space LiDAR applications.

*eric.deborniol@cea.fr

The optimization of the HgCdTe APD technology and an overview of the new ROIC development has been reported in a previous paper[4]. In this first version of detection module, the ROIC was indium bump hybridized to the HgCdTe APD as it is usually done for HgCdTe focal plane arrays. This photodiode/ROIC coupling scheme requires a specific CMOS processing which imposes to fabricate a full dedicated wafer batch. A second version of the ROIC that can be coupled to the APD by wire bonding was designed and included in the specific CMOS batch realized for the first version. This version of the ROIC has the same features as the previous one. There are two main advantages of such a coupling scheme: first the ROIC can be coupled to an APD with arbitrary geometry and do not need to be adapted to the CMOS circuit, second the ROIC can be fabricated on a multi-project CMOS wafer manufacturing. This second point allows reducingthe development time and costs, to optimize and/or to adapt its design to specific application needs. This paper will focus on the test results obtained on detector module using this second APD/ROIC coupling scheme.

The ROIC design and main features as the detailed architecture of the two versions of detector modules, hybridized and wire bonded based on this circuit are presented in section 2. The first characterization results from a HOLDON detector module made by wire bonding are reported in the section 3. The last section presents the conclusion and perspectives that can be made from the results of this study.

2. DETECTOR DESIGN AND DEVELOPMENT

2.1 ROIC design

The main challenge for HOLDON ROIC design was to find an architecture enabling a linear detection that can handle more than 6 order of magnitudes of incoming photonic flux and at least 2 order of magnitudes in temporal resolution with a sensitivity close to the single photon level. The high dynamic range could only be achieved by implementing a variable gain amplifier. Two main configurations were considered, resistive trans-impedance amplifier, RTIA, and capacitive trans-impedance amplifier, CTIA. An analysis of both configurations evidenced that CTIAs allow a more stable operation for a larger variation in feedback gain. In addition, the Johnson noise of the resistance in RTIAs gives an increased noise at higher gain values that limits the gain in sensitivity.

For a CTIA based photodetector, the output signal corresponds to the integral of the detected photocurrent (cf. Figure 1). The detection of a photon pulse is translated into a star-case signal proportional to the number of detected photons. A reset of the feedback capacitance, driven by “raz” logical signal in Figure 1, is therefore needed to avoid a saturation of the circuit. The electronic gain change is made by a variation of the feedback or integration capacitance, C_{int}. A reduction of the feedback capacitance will induce an increased reset noise. But this reset noise is only a variation of an offset voltage for each recorded waveform (a waveform being here the voltage integration ramp from one reset to the next one) that can be easily eliminated by using data treatment based on a derivation of the recorded signal.

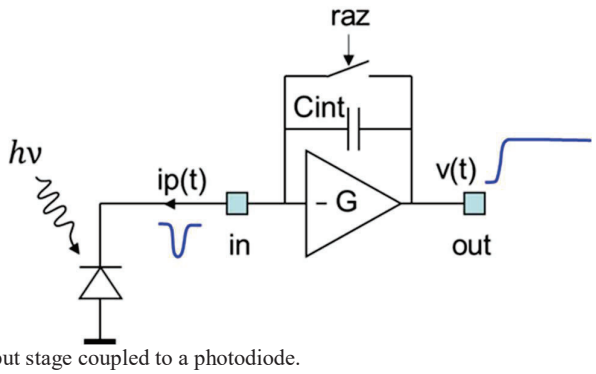

Figure 1 . CTIA electronic input stage coupled to a photodiode.

As already mentioned, the main drawback of the CTIA input stage architecture is that the charge integration on the capacitance can saturate in case of the detection of strong signals. For LiDAR applications, this requires a good knowledge

of the temporal photonic signal evolution scenario to adapt the gain and/or to insert a reset during the reception of the signal. To avoid saturation, the ROIC gain can be dynamically changed during the observation by switching from a high to a lower gain. The reset is also an option but it will introduce a dead time with a loss of data that need to be positioned in a region of expected low interest. This reset dead time is expected to be lower than 50 ns. To cope with the case of limited knowledge on the temporal variation of the LiDAR signal, we have also implemented an automatic reset function. It resets the capacity once a given (user defined) signal level has been obtained. This functionality allows avoiding a long dead time after saturation but might introduce reset dead-times at variable instants of time that might introduce important loss of information.

The ASIC amplification chain is presented in Figure 2. The signal from the CTIA can be output from the ASIC using two modes of operation. The first, illustrated in Figure 2 a, is termed the continuous mode. In this mode, the signal is subject to an optional filtering before being directly amplified with a buffer that enable to charge the output with a impedance down to 50 Ohm. The output can be single ended with signal range of 2.4 V, or differential, with a signal range of 4.8 V when charged on high impedance. The latter can favorably be used to suppress common mode fluctuations and is directly compatible with differential input ADCs.

In the second mode, termed on chip sampling (OCS) and illustrated in Figure 2 b), the CTIA output signal is sampled in the ROIC. The analog samples are stored on 2048 capacitors. An external LVDS clock controls the sampling time (write/read clock). The sampling frequency can be adapted to the expected waveform of the LiDAR signal with asynchronous rate up to 100 Msamples/s. The recorded samples are then sequentially read-out at a slower rate controlled with the LVDS signal. This enables to use an ADC with slower sampling rate associated with higher number of bits and larger dynamic range. The reduced bandwidth on the signal at the output of the buffer in the OCS mode does also allow to increase the charge at the input of the external sampling unit, that is expected to increase the linearity of the buffer amplifier.

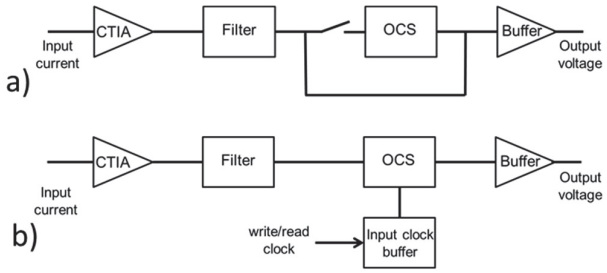

Figure 2 . HOLDON ROIC modes of operation. a) In continuous mode, the output of the CTIA is directly accessible at the output. b) In the On Chip Sampling (OCS) mode, the signal is first sampled at high rate within the ROIC and sequentially read at a lower rate in order to use low noise, high resolution and high dynamic ADC.

In order to meet the large dynamic range needed for LiDAR we have implemented 4 different gain values, each time varied by one order of magnitude, ranging from 10 fF to 10 pF. The ROIC was made using the H9AROIC CMOS technology from STMircroelectronics. This process has a 130 nm resolution and thick oxide that sustain a maximum voltage of 4.8 V. This high voltage is in favor of large linear dynamic range for each gain. Preliminary simulation has shown a linear range of 2.4 V for each gain setting. Table 1 resumes the expected performance in terms of signal range, noise and linearity for the different CTIA gains. A very low noise is expected at all gains and allows a dynamic range up to 92 dB in electrical power ratio for the two highest gains. This high dynamic range is combined with a down to single photon level detection when associated with an APD gain in excess of 100 at the two lowest gain settings G1 and G2.

Table 1. Expected characteristics of the versatile HOLDON ROIC. The dynamic range is expressed in electrical power ratio.

Gain	C (fF)	Signal range (V)	Charge capacity (Melectrons)	Noise (µV)	Electron noise rms M=1	Electron noise rms M=100	Dynamic range (dB)	Full range linearity fluctuations (%)	BW (MHz)
G1	10	2.4	0.15	390	24.3	0.2	75.8	2	3
G2	100	2.4	1.50	90	56.2	0.6	88.5	0.2	30
G3	1000	2.4	14.98	60	374.5	3.7	92.0	0.04	300
G4	10000	2.4	149.81	60	3745.3	37.5	92.0	<0.01	300

The expected linearity for a given feedback capacity is strongly dependent on the gain of the CTIA, mainly through the variations of parasitic capacitances that have a strong voltage dependence. This result shows that the APD gain is not only useful to reduce the impact of the amplifier noise but does also increase the linearity of the amplifier as it allows to integrate a small signal on a larger capacitance. For example, the G1 at unity APD gain and the G4 at a gain of 100 are characterized by a similar input noise, but the linearity has been improved by 2 orders of magnitudes using the APD gain. This feature could be of high importance for the most demanding LiDAR applications.

2.2 Detector modules assembly

Based on the architecture described in the previous section, two version of the ROIC were design and realized on the same CMOS batch. A first version, named CL111, is designed for indium bum flip chip hybridization between MCT APD and ROIC. The other ROIC, CL112, is made to do this connection by simply wire-bonding the APD to dedicated pads of the ROIC. In that case, the photodiode array is first hybridized to an interconnection circuit used to form APD macro-pixels. The interconnection circuit/APD module can then be tested and coupled to the ROIC by wire bonding. With the hybridized detector, the APD array himself cannot be tested before being associated to the ROIC. This early test and selection of APD module is the first advantage of this wire-bonding scheme. The other one is the fact that wire-bondable ROIC can be realized on multi-project CMOS wafers. This is much less expansive and easier to access CMOS process allowing to explore different ROIC architectures options for a given application or to make evolution of existing one. However, the ultimate performances in terms of noise and bandwidth are more likely to be obtained with an hybrid detector module.

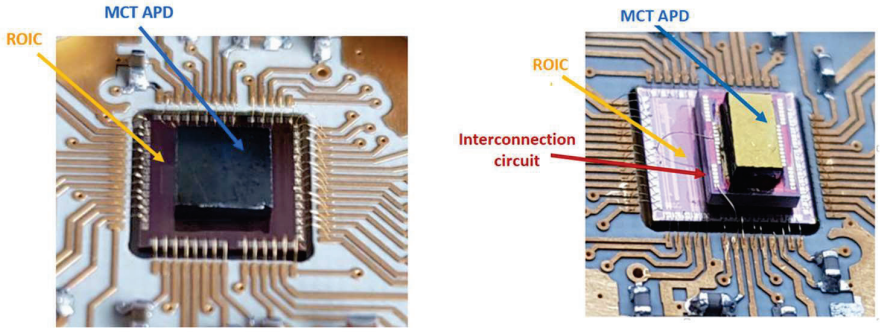

Figure 3 . a) hybrid detector module based on indium bump flip chip hybridization between MCT APD and ROIC CL111; b) wire bonded detector module: the photodiode is hybridized to an interconnection circuit and connected to a specific input pads of the ROIC CL112.

The wire-bonded module used in this study is made of 76 photodiodes at 15 µm pitch forming a 150 µm diameter APD macro-diode. In both cases, CL111 or CL112 based detector modules, the ROIC is wire bonded to a dedicated cold PCB before being integrated in the HOLDON cryostat.

3. ELECTRO OPTICAL TEST RESULTS OF A BONDED MODULE

3.1 Test setup

Figure 4 shows a block diagram of the detector's test setup. The detector module were tested using 1.55 µm fiber coupled lasers. For static measurements we used a continuous laser and for dynamic measurement a pulsed laser. The pulsed one is a GSL model laser from CALMAR having a pulse width in the tens of picosecond range. The laser pulse energy is controlled via a variable optical attenuator (VOA) from JGR. The attenuation range goes from 0 to 100 dB with 0.1 dB accuracy or 2.3 %. The mean pulse power at the output of the fiber can be measured via a power meter. A simple optical system made of two lenses allows imaging the fiber output on the detector collecting all the photonic flux. The detector module is operated at 80 K thanks to a passively cooled cryostat. A F/4 cold aperture and 2.4 µm cold low pass filter are implemented inside the cryostat to limit the thermal background photonic flux.

The ROIC was controlled using a dedicated proximity electronic card that was developed at CEA/Leti and a generic low noise bias supplies and clock generators usually used to control infrared focal plane arrays. The signal was sampled using a 12 bit Tektronix MSO6 oscilloscope. The oscilloscope was most of the time operated with a sample rate of 625 MS/s allowing to get 16 bits of vertical resolution. This high-resolution mode reduces the oscilloscope input noise. This feature was very useful to measure the 60µV ROIC noise expected for the two lower CTIA gains. An arbitrary generator function AFG 3102 from Tektronix, which is not depicted Figure 4, perform synchronization of all signals controlling the laser and the detector.

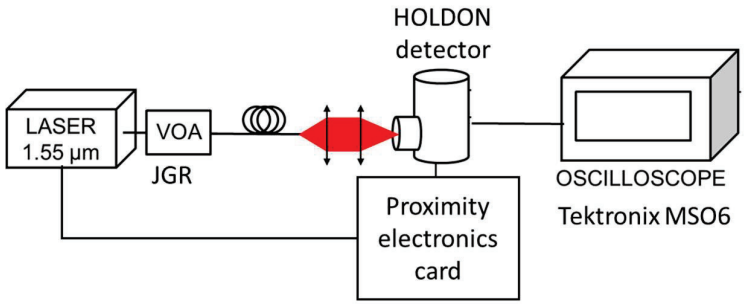

Figure 4 . HOLDON modules test bench.

3.2 Electro-optical performances of the wire bonded detector

As for the hybrid version of detection module, the auto-reset and internal switchable low pass filters of the ROIC were found to be functional. The reset dead time is unchanged at 50 ns. The OCS mode of operation is also functional. Saying that, the results reported here after were acquired in continuous mode. The output buffer has a positive and a negative output to be able to provide a differential signal to the following part of the data acquisition chain. During these measurements, we only used the positive one, OutP, loaded on the high impedance entrance of the oscilloscope.

A first series of measurements were made with the continuous laser. From these measurements, we will evaluate the values of the ROIC feedback capacitance, the quantum efficiency and the APD gain. Another series of measurements needing the pulse laser were performed. We then get the evaluation of the quantum efficiency to excess noise ratio (QEFR), the detector bandwidth and the dynamic and linearity figure of merit. Without any voluntary incoming flux, there is still a residual photocurrent due to the thermal background photons. The background current and associated noise give us information about the detector performances that can be obtained in practice with our optical aperture configuration. To get an idea of the ultimate noise that can be obtained we also made some measurements in dark conditions by setting an obstructed cold aperture in front of the detector.

Continuous laser measurements

The value of the four integration capacitances of the wire-bounded module were re-evaluated. The 10 pF, G4, value is calculated from the measurement of the total photocurrent flowing to the APD anode (via the dedicated ROIC bias) when the detector is illuminated by the continuous laser. The voltage drop for a given time of integration gives a direct measure of the capacitance. This method of C_{int} value evaluation supposes that none of the photodiodes array forming the sensitive surface have an excessive dark current (what was checked later). Otherwise, the value obtained by this way takes into account all the gains applying along the measurement chain. It is the effective conversion gain to be taken into account for Volt to electron conversion. In the rest of the document, we used C_{int} for clarity, even if it is not the real value of the feedback capacitance. By convention, to talk about the used ROIC gain, we use the designed instead of the measured one. In the measurement process, the 1 pF C_{int} value is inferred from the 10 pF one thanks to the measure of the ratio of their integration slope at a given flux. The 100 fF is again inferred from the ratio of slope with the 1pF and so on. We used this method as the direct measurement of weak current presents larger uncertainties than bigger ones.

Table 2. Designed and measured ROIC capacitances values.

Elec. Gain	Cint design.	Cint éval.	Ratio to prev.
i	fF	fF	G_{i+1}/G_i
G4	10 000	9 500	-
G3	1 000	962	9.87
G2	100	110	8.76
G1	10	12	9.44

The APD gain curve is depicted Figure 5. It was measured using the G4 ROIC capacitance. A gain of 78 is obtained for 11.4 Volt of APD reverse bias voltage.

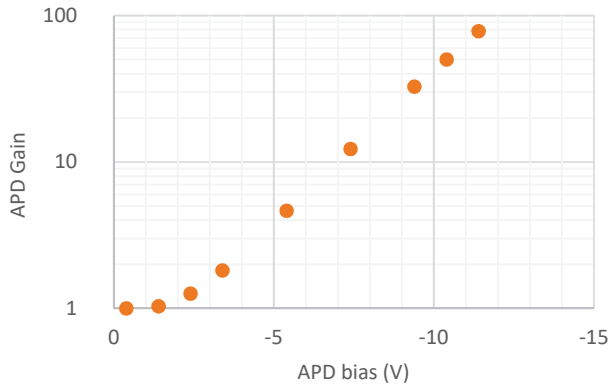

Figure 5 . Measured APD gain curve of Holdon detector module.

Pulsed laser measurements

Knowing the value of the ROIC conversion gain, C_{int}, we can evaluate the **quantum efficiency** (QE) at unity APD gain. The number of photons per laser pulse is measured using a power meter at the output of the optical fiber, before the optics. The number of electrons produced by the pulse is measured via the voltage step amplitude produced by the laser pulse at the ROIC output. We have used the 100 fF CTIA gain and made the number of electron calculation with the corresponding measured value of 110 fF. The resulting QE is 70%.

We have also evaluated the quantum efficiency to excess noise ratio, **QEFR**, and the excess noise factor, F. The value is obtained from the signal to noise ratio measured for 1000 successive laser pulses compared to the theoretical one calculated

from the known number of incoming photons per laser pulse. This has been done at the maximum APD reverse bias voltage that we used (11.4 Volt) with the 100 fF C_{int}. The laser is attenuated (to about 300 photons per pulse) in order to reduce the pulse to pulse amplitude fluctuations coming from the laser himself. We get a QEFR of 0.53 and so an F value of 1.28. The QE and QEFR results are a bit lower than excepted. It can be attributed to the use of the "historic" CEA/Leti APD technology, with small area APDs on a small pitch that forms a large area macro diode in which the QE and excess noise are limited by the diffusion collection and multiplication layer inhomogeneity. Furthermore, these values assume a 100 % transmission of the optics (collimating and focusing lenses, cryostat window and optical cold filter). The real values of QE and QEFR can only be higher.

The dynamic range of the CL112 ROIC was measured at unity APD gain using the pulsed laser and the variable optical attenuator (VOA). The number of photons per pulse is measured with a power-meter for the lower optical attenuation and then inferred from the applied attenuation set for lower pulse energy values. The dynamic measurements results are presented Figure 6 a. For the two biggest capacitances, we used a multi-pulses scheme to reach the high number of photons needed to reach the top of the dynamic range. If we take into account the maximum value of measured APD gain, the values at the top of the dynamic reaches $2x10^6$ photons. With a raw input noise of 0.9 photons measured for this APD gain (result of the background noise measurements for C_{int} = 10 fF presented later), the total shot noise limited dynamic range overcomes the initial project goal of 10^6.

The linearity over this dynamic was evaluated from the same set of data. The non-linearity (NL) plotted Figure 6 b is the relative deviation to the data linear fit. In order to cover the wide dynamic range, the measurement is made with an exponential progression of the laser pulse energy. To keep an equivalent weight to each measurement the fit is realized on the log of the photon number and resulting voltage deviation. For the gains G2 to G4, the non-linearity values are found to be contained within the precision of the VOA (+/- 2.3 %). The non-linearity is higher for G1 (C_{int} = 10 fF). A stronger non-linearity for this gain was also found during the simulations of the ROIC, although the experimental values are a factor 4 higher. Supposing this ratio is true for the other gains, the corresponding non-linearity is expected to be lower than 1 % at G2, below 0.1 % at G3 and about 0.01 % at G4.

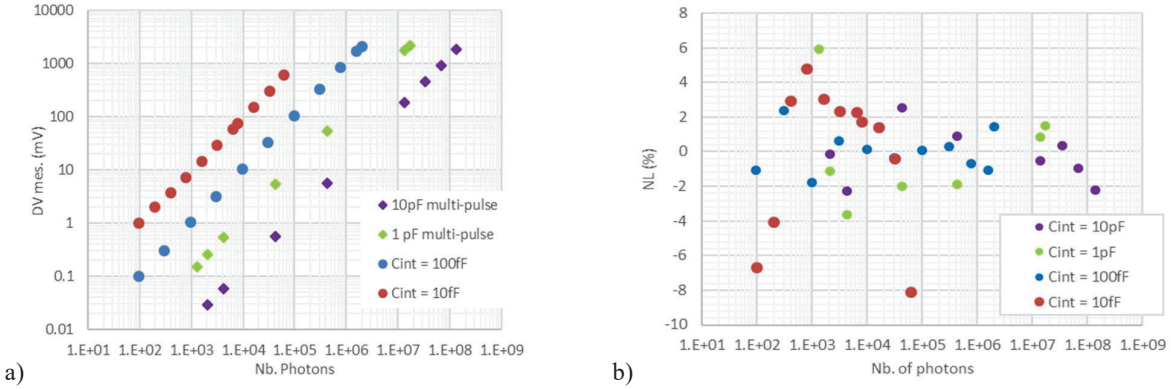

a) b)

Figure 6 . Dynamic range measurement (a) and calculated non-linearity (b).

The bandwidth of the detector was evaluated by measuring the rise time of a laser pulse on OutP. Table 3 gives the measured rise time (τ_r, from 10% to 90% of the pulse swing) and the corresponding bandwidth for a SubPV bias of -2.0 V. These values allow responding to most of the atmospheric LiDAR applications in which the duration of the laser pulses are rarely below 10 ns. We have observed that the rise time can be improved by about 20% by forcing a specific bias of the ROIC at a higher value (2.0 V instead of 1.5 V). For the 1 pF C_{int} we get a rise time of 6 ns instead of 8.4 ns. The reported values and corresponding bandwidth are slower than the one measured on a similar APD (BW = 175 MHz, τ_r = 2 ns). This indicates that the slow response of the detector is due to a limitation within the HOLDON ROIC. The origin of this limitation has not yet been determined. A possible origin can be the modification of the performance at low operating temperature of the large area transistor at the input stage of the ROIC.

Table 3. Detector rise time and bandwidth (measure).

ROIC Gain	C	Rise time	BP
	F	ns	MHz
G4	10 p	6	58.3
G3	1 p	8.4	41.7
G2	100 f	20.6	17.0
G1	10 f	175	2.0

Measurements under background or residual photonic flux

The background current evolution with the APD bias and its value normalized by the corresponding measured APD gain are plotted Figure 7. Residual background current in laboratory conditions is around 1pA. This corresponds to a background signal of 8.6×10^6 photons/s. This value is lower than the background expected in most space LiDAR scenarios.

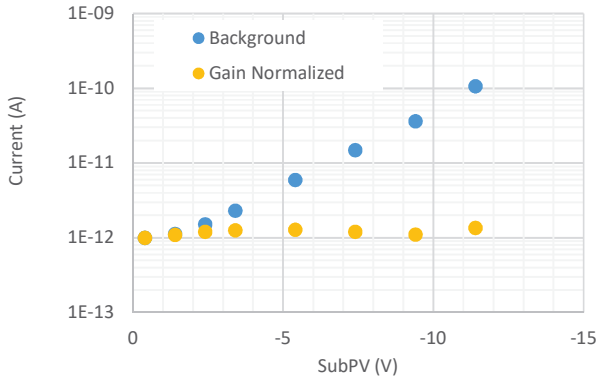

Figure 7 . Background current measured on the detector module D3 (HOLDON 2201) equipped with a cold optical aperture of F/4 and an IR blocking cold low pass optical filter.

The noise under background flux was evaluated for each CTIA gain with and without APD gain. Given that the implementation of a CTIA input stage in the HOLDON ROIC would require a signal processing adapted to each application scenario, we have evaluated the noise on different time scales and for different signal processing schemes:

- The RAW noise: computation of the standard deviation under a given period (*dt*),
- The CDS (for Correlated Double Sampling) noise: standard deviation of the difference between two samples separated by *dt*.
- The Fowler noise: standard deviation of the Fowler signal. To get that signal the record samples are averaged during *dt/2* at the beginning and the end of the time interval, *dt.* We then compute the difference of the averaged samples, as for the CDS.

The results are expressed in µV at the ROIC output, in number of electrons at the CTIA entrance and in photons at the detector input by taking into account the QE and APD. The results for APD gain of 78 and a time interval, *dt*, of 205 ns are given Table 4. The oscilloscope noise used was subtracted to get the real detector performances. The ROIC noise is included on these noise results. The raw input noise goes down to less than 1 photon for the higher ROIC gain.

Table 4. Background noise measurement results for an APD gain of 78 and *dt* = 205 ns.

C	Raw	CDS	Fowler	Unit
10 fF	678.0	1531.0	1334.0	µV
	49.3	111.3	97.0	e-
	0.9	2.1	1.8	ph
100 fF	181.5	311.7	187.1	µV
	124.6	213.9	128.4	e-
	2.3	4.0	2.4	ph
1 pf	64.9	89.0	28.5	µV
	390.2	535.2	171.6	e-
	7.3	10.0	3.2	ph
10 pF	60.1	76.1	18.7	µV
	3570.4	4520.9	1112.5	e-
	66.7	84.5	20.8	ph

For these measurements, *dt* was fixed to 205 ns to be in the range of the detector measured response time for the highest ROIC gain. This time interval also has an influence on the detector noise. This is illustrated Table 5 where different time intervals were used for the 100 fF C_{int} record. The observed increased raw and CDS noises at the longest observation times can be explained by the shot-noise on residual background light.

Table 5. Background noise measurement results for C_{int} = 100 fF as a function of time interval *dt*.

dt (ns)	Raw	CDS	Fowler (dt/2)	Unit
20.8	116.5	231.5	199.6	µV
	79.9	158.9	137.0	e-
	1.5	3.0	2.6	ph
41.6	146.6	266.5	218.5	µV
	100.6	183.0	150.0	e-
	1.9	3.4	2.8	ph
204.8	181.5	311.7	187.1	µV
	124.6	213.9	128.4	e-
	2.3	4.0	2.4	ph

Dark conditions measurements

The dark current was evaluated by setting an obstructed cold screen (thermally connected to the cryostat cold finger) in front of the detector. This measurement demonstrates the ultimate performance level of the presently used APD, although some residual photons might still leak onto the detector. The evolution of the measured value with the APD bias voltage is displayed Figure 8. At the highest APD gain, the dark current is about 20 pA. Divided by the APD gain it gives 1.6×10^6 e-/s. This corresponds to the lowest signal level considered for the atmospheric LiDAR scenarios during the first period of the HOLDON project.

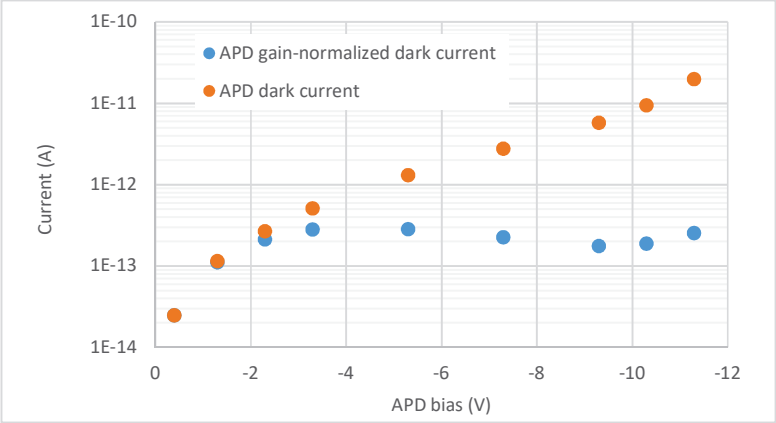

Figure 8 . Dark current measured on the detector equipped with an obstructed cold screen (C_{int} = 100 fF).

The dark noise was also measured for the highest APD gain. The results obtained for *dt* = 205 ns are summarized . It can be seen that the noise is reduced compared to the one reported in Table 4, corroborating the conclusion that the increased noise in background condition measurements is due to the detection of residual background flux.

For the smallest capacitance, the raw noise is below one photon (0.57 photons), showing the capacity to use the HOLDON detector in photon counting mode at only a slightly higher gain in excess of 100. At G2 (C_{int} =100 fF), the observed performance is still close to the photon counting limit, with a raw noise at the level of a single photon. CDS and Fowler noise are slightly higher due to the integration of the APDs dark current and to the ROIC noise addition occurring when samples are substracted. The raw noise values measured at the circuit output are very close to the excepted ones extracted from the ROIC simulations and listed Table 1.

Table 6. Measured noise in dark conditions for an APD gain of 78 and *dt* = 205 ns.

C_{int}	Raw	CDS	Fowler (dt/2)	Unit
10 fF	419.2	1 000.25	874.08	µV
	30.5	72.7	63.6	e-
	0.57	1.36	1.19	ph
100 fF	81.2	199.58	129.39	µV
	55.7	137.0	88.8	e-
	1.0	2.6	1.7	ph
1 pF	66.6	81.71	28.60	µV
	400.6	491.4	172.0	e-
	7.5	9.2	3.2	ph
10 pF	51.5	77.65	23.09	µV
	3 060.0	4 610.7	1 370.9	e-
	57.1	86.1	25.6	ph

3.3 Persistence measurement and results

Differential absorption LiDAR (DIAL) or Bathymetric LiDAR measurements gives rise to signal with a high photon flux level followed by a more or less rapid decay[5]. The knowledge of the detector persistence is therefore essential for the end users.

We have evaluated the detector persistence for different scenarios of use of the ROIC. In the first case, we select a CTIA feedback capacitance and send a laser pulse giving an output step finishing in the top of the ROIC dynamic. In a second case of use, we send the same amount of photon per pulse but we change the ROIC feedback capacitance from a higher value when the pulse is received to a lower one to keep a good sensitivity. During these measurements, we used the 100 fF C_{int} value as reference and 10 pF as first value of CTIA gain when using the C_{int} switch protocol. The data treatment applied in that case was the previously explained Fowler sampling with a *dt* = 21 ns. This *dt* value is equivalent to the 100 fF response time giving an optimal signal to noise ratio on Fowler data. All the presented persistence results are normalized to get a unity laser pulse step on the 100 fF C_{int}. The test were made at -2V of APD bias. The signal used to compute the persistence is the average of 1000 successive records in order to reduce the temporal noise.

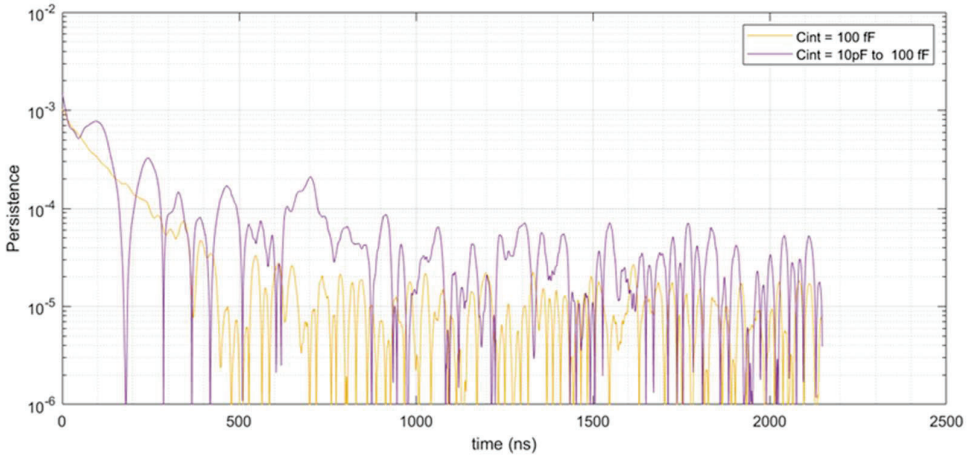

Figure 9. Relative persistence on the Fowler(*dt* = 21ns) signal measured in two case of ROIC gain management: with a fixed C_{int} of 100 fF and when setting it at 10 pF during laser pulse arrival and changing it to the 100 fF 65 ns after the pulse to enhance the ROIC sensitivity. The plot starts at this instant, 65 ns after the laser pulse in both cases.

An example of the persistence measurement result with and without ROIC gain change after the laser pulse is depicted Figure 9. The plot start at the instant of C_{int} change, 65 ns after the laser pulse when apply. After 250 ns, the relative persistence reaches 10^{-4}. During the first 400 ns, the decay is equivalent for both ROIC gain management strategies but with a more stable signal when changing the C_{int} value after the laser pulse. The residual temporal noise of the detector limits the measure of the C_{int} change case to about 10^{-5}. The value of 10^{-5} is obtained after 500 ns in the C_{int} change case but with a less stable signal. This value is reached later for fixed C_{int} value. As the ROIC bandwidth is very different for the two capacitances, the similar initial decay lets us think that the photodiode is at the origin of the persistence. Finally, changing the ROIC gain allows to get the higher sensitivity of the 100 fF gain with the lower associated noise without the signal fluctuation observed when the ROIC gain is fixed.

Another situation is the case where the laser pulse would have saturated the ROIC with the small capacitance. This case required a ROIC gain change to be able to record the pulse. We have done that with a laser pulse of about $3x10^6$ photons (3 times more than for the non-saturated test). We observe the same decay as before but thanks to a lower noise plateau we can measure the persistence down to a few 10^{-6} (cf. Figure 10). This lower plateau observed in this case comes from the fact that we normalize the record by a higher laser pulse amplitude.

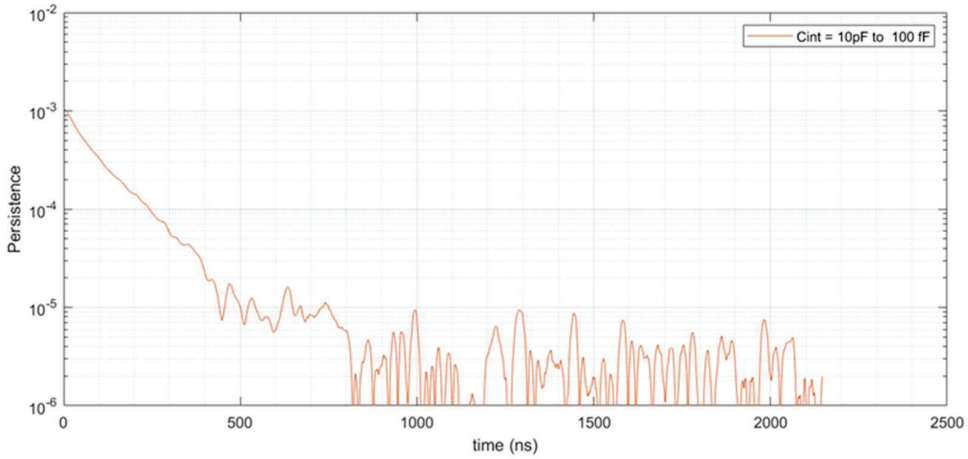

Figure 10. Relative persistence on the Fowler (dt = 21ns) signal with C_{int} changed from 10 pF to 100 fF and 3x10^6 photons laser pulse. This pulse energy would have saturated the ROIC for 100 fF C_{int}. The plot starts at the C_{int} change time and the laser pulse occurs 65 ns before.

4. CONCLUSION AND PERSPECTIVES

We have tested a wire-bonded version of the versatile HOLDON detector dedicated to LiDAR applications. Electro optical test results obtained with the bonded version of the detector show that the performances are very similar to what we get with the hybrid version. This significant result allows us to continue ROIC developments without having to pay for and/or wait for the realization of a complete dedicated CMOS wafer batch.

In terms of electro optical performances, at the highest photodiode bias that we have tested we get an APD gain of 78 with an excess noise ratio of 1.28. The quantum efficiency is higher than 70 %. The expected high linear dynamic range of more than 6 orders of magnitudes has been reached thanks to the variable CTIA gain. This high dynamic range is associated with a high sensitivity as the raw ROIC noise was measured under the single photon for the higher ROIC gain and the maximum APD gain. The best value of rise time that was obtained is 6 ns. Even if it is more than expected, it is far enough for most of the expressed needs for LiDAR instruments where the laser pulse is at least 10 ns. The gain normalized dark current is at 1.6x10^6 e-/s. This value is equivalent to the lowest value that was considered during the first period of the HOLDON project dedicated to the different LiDAR scenarios definition. We have experimentally demonstrated that the relative persistence is at 10^{-5} after 500 ns after a large photonic pulse and it continues to decrease after, the measure of the final value being limited by our experimental set-up. We have also shown that changing the ROIC gain just after a photonic pulse leads to a more stable decay of the persistence signal.

In a short-term, we will test, and deliver to our partners, detector modules using micro lenses to enlarge the effective detector area while keeping a small active APD.
In a mid-term perspective, the HOLDON detector will benefit from our ongoing development of the APD technology leading to a larger gain, lower excess noise and higher bandwidth[6][7].

ACKNOWLEDGEMENTS

This work was supported by the CNES and the European Union's Horizon 2020 research and innovation program under grant agreement no 776390.

REFERENCES

[1] Rothman, J., "Physics and Limitations of HgCdTe APDs: A Review," J. Electron. Mater. 47, 5657–5665 (2018).
[2] Monica Rodríguez Cortina, Pawel Adamiec, Juan Barbero, Xabier Quintana, Morten Andreas Geday, "Development of a NIR-VIS-UV LiDAR echo emulator," Proc. SPIE 11852, International Conference on Space Optics — ICSO 2020, 118526F (11 June 2021); https://doi.org/10.1117/12.2601249.
[3] Pawel Adamiec, Alvaro Machon, Monica Rodriguez Cortina, Alejandro Lopez Moya, Enrique Cordero, Juan Barbero, "LiDAR echo emulator," Proc. SPIE 11180, International Conference on Space Optics — ICSO 2018, 111801U (12 July 2019); https://doi.org/10.1117/12.2535985.
[4] J. Rothman, E. De Borniol, S. Pes, A. Dumas, B. Hoareau, S. Renet, L. Mathieu, J.-A. Nicolas, J.-P. Rostaing, J. le Perchec, G. Badano, P. Bleuet, P.Castelein, J. Abergel, S. Gout, X. Baudry, P. Ballet, J.-L. Santailler, "HgCdTe APDs detector developments for high speed, low photon number and large dynamic range photo-detection," Proc. SPIE 11852, International Conference on Space Optics — ICSO 2020, 118520F (11 June 2021); doi: 10.1117/12.2599159.
[5] A. Dumas, J. Rothman, F. Gibert, D. Édouart, G. Lasfargues, C. Cénac, F. Mounier, J. Pellegrino, J. Zanatta, A. Bardoux, F. Tinto, and P. Flamant, "Evaluation of a HgCdTe e-APD based detector for 2 µm CO_2 DIAL application," Appl. Opt. 56, 7577-7585 (2017).
[6] J. Abergel, S. Gout, A. Coquiard, L. Lechevallier, F. Berger, S. Renet, G. Lasfargues, A. Vandeneyde, S. Brunet-Manquat, G. Badanoa, A. Dumas, E. Massit, D. Giotta, J.-L. Santailler, J. Rothman, " High operating HgCdTe APDs for free space optical communications", Presented at International Conference on Space Optics -ICSO 2022 (2022).
[7] J. Rothman, S. Pes, J. Abergel, S. Gout, A. Coquiard, G. Badano, G. Lasfargues, A. Vandeneyde, J.-A. Nicolas, J.-L. Santailler, "HgCdTe APD detector module for deep space optical communications", Presented at International Conference on Space Optics -ICSO 2022 (2022).